

# Evaluation of snow depth retrievals from ICESat-2 using airborne laser-scanning data

César Deschamps-Berger<sup>1,2</sup>, Simon Gascoin<sup>1</sup>, David Shean<sup>3</sup>, Hannah Besso<sup>3</sup>, Ambroise Guiot<sup>1</sup>, Juan Ignacio López-Moreno<sup>2</sup>

5 <sup>1</sup>Centre d'Etudes Spatiales de la Biosphère, CESBIO, Univ. Toulouse, CNES/CNRS/INRAE/IRD/UPS, Toulouse, France.

<sup>2</sup>Instituto Pirenaico de Ecología, Consejo Superior de Investigaciones Científicas (IPE-CSIC), Zaragoza, Spain.

<sup>3</sup>University of Washington, Dept. of Civil and Environmental Engineering, Seattle, WA.

*Correspondence to:* César Deschamps-Berger (cesar.deschamps-berger@csic.es)

10 **Abstract.** The unprecedented precision of the altimetry satellite ICESat-2 and the increasing availability of high-resolution elevation datasets open new opportunities to measure snow depth in mountains, a critical variable for ecosystems and water resources monitoring. We retrieved snow depth over the upper Tuolumne basin (California, USA) for three years by differencing ICESat-2 ATL06 snow-on elevations and various snow-off ~~elevation sources, including ATL06 and external~~ digital elevation models. Snow depth derived from ATL06 data only (snow-on and snow-off) ~~would provided~~ a poor  
15 temporal and spatial coverage, limiting its potential utility. However, using airborne lidar ~~or satellite photogrammetry~~ elevation models as snow-off elevation source yielded an accuracy of ~0.2 m (bias), a precision of ~0.5 m ~~for low slopes and ~1.2 m across the basin and an improved precision of 0.5 m for low slopes steeper areas~~, compared to eight reference airborne lidar snow depth maps. Snow depths derived from ICESat-2 ATL06 and a satellite photogrammetry elevation model have a larger precision and bias, partly induced by forested areas. These various combinations of repeated ICESat-2 products with satellite or airborne products, will enable tailored approaches to map snow depth and estimate water resources in yet poorly monitored regions. The snow depth derived from ICESat-2 ATL06 will help address the challenge of measuring the snow depth in unmonitored mountainous areas.  
20

## 1 Introduction

25 Seasonal snow ~~cover~~ provides fresh water resources to over a billion people globally (Barnett et al., 2005; Sturm et al., 2017). The spatial distribution of the mass of snow on the ground (snow water equivalent, SWE) in snow dominated catchments is key information to predict runoff during the melt season (Freudiger et al., 2017). Yet, direct mapping of the SWE in mountains remains technologically challenging (Dozier et al., 2016). Recent studies have shown that the assimilation of remotely sensed snow depth data is a viable method for estimating SWE spatial distribution ~~as the SWE can~~  
30 ~~be calculated from the snow depth and the snow density~~ (Brauchli et al., 2017; Margulis et al., 2019; Deschamps-Berger et

al., 2022). ~~of societal or ecological interest, typically larger than 100 km<sup>2</sup> (National Academies of Sciences, Engineering, and Medicine, 2018).~~ Efforts are made to address the challenge to map the snow depth in mountainous catchment. Several methods are nowadays available to map snow depth in mountainous catchments of societal or ecological interest, typically larger than 100 km<sup>2</sup>. Calculating the difference between a snow-on and snow-off digital elevation model (DEM) is one of the most straightforward methods. Snow-on and snow-off DEMs can be derived from airborne lidar or photogrammetry with resolution and vertical precision of 10-30 cm (Deems et al., 2013; Bühler et al., 2015). ~~With the Airborne Snow Observatory (ASO), several snow dominated catchments of more than 1000 km<sup>2</sup> are monitored with airborne lidar about every two weeks during the melt-period in California and Colorado, USA. The 3 m resolution snow depth maps have an uncertainty of ~0.1 m (Currier et al., 2019; Mazzotti et al., 2019) and are assimilated in a snowpack model at a lower resolution of 50 m, providing accurate and temporally continuous SWE estimates (Hedrick et al., 2018).~~ However, these flights are expensive, and repeat snow-on flights are only available in a few basins globally. ~~Basins with extensive ASO data are ideal for testing new snow depth detection methods.~~ An alternative to airborne campaigns is to compute DEMs from very-high-resolution stereoscopic satellite images (i.e. photogrammetric method). Snow depth maps at a resolution of 2-3 m were produced from images of the Pléiades or WorldView constellations with an uncertainty of ~0.70 m (Marti et al., 2016; Shaw et al., 2019; McGrath et al., 2019; Deschamps-Berger et al., 2020; Eberhard et al., 2021). The orbits of these satellites enable the imaging of any region of the Earth's surface (cloud-permitting) but the on-demand acquisition mode results in a discontinuous archive in time and space. Based on a different physical approach, ~~S~~ snow depth maps have been retrieved from Sentinel-1 ~~observations~~ backscatters by calibration with snow depth measurements at automatic weather stations (Lievens et al., 2019; Lievens et al., 2022). A single global calibration factor yielded an error of ~2 m (mean absolute error) at 250 m resolution. With the 12 day revisit of Sentinel-1, this approach provides frequent acquisitions globally at an intermediate spatial resolution. However, this method is not applicable during the melt season when the radar signal is absorbed by the liquid water contained in the snowpack.

Spaceborne lidar missions measure elevation along linear tracks parallel to the satellite orbit. The NASA Ice Cloud and Land Elevation Satellite (ICESat) GLAS instrument was operational from 2003 to 2010 and measured the elevation along a single track every 170 m within a footprint of 70 m. Snow depth could be retrieved from ICESat snow-on observations using a reference airborne lidar snow-off DEM (Treichler et al., 2017). At the footprint scale, the snow depth uncertainty reached an RMSE of 1 m. Due to the sampling structure and the accuracy of ICESat, snow depth data were sparse and not retrieved over slopes greater than 10°. This method was best suited to measure snow depth averaged over seasons and elevation bands, which means a coarsening of the temporal and spatial resolution. Since October 2018, the higher resolution follow-up mission ICESat-2 has provided improved elevation measurements using ATLAS, a photon-counting lidar instrument. The tracks of ICESat-2 consist of three pairs of a strong and a weak beam each, with a cross-track distance of 3.3 km between pairs and 90 m between beams. The photon pulses are spaced by ~0.70 m along-track and illuminate an area of ~11 m in diameter (Markus et al., 2017; Smith et al., 2019) with geolocation accuracy of ~3-4 m (Magruder et al., 2021). However, the orbit of ICESat-2 was designed to increase the spatial density of the tracks coverage for biomass applications in the mid-

65 latitudes. Thus, outside of the polar areas, the tracks are offset and rarely perfectly overlap, which precludes a straightforward approach of retrieving snow depth by differencing snow-on and snow-off elevations along every ICESat-2 transect. The individual photon returns, i.e. the raw products, are processed to provide, for instance, estimates of land ice elevation changes with a 20 m spacing along track (ATL06) or forest canopy height at a 100 m spacing (ATL08). Other applications have emerged, including attempts to measure snow depth with ATL08 and ATL06 (Hu et al., 2021; Enderlin et al., 2022). ~~However, this application is challenging since ICESat-2 was not designed to make frequent repeat measurements at the same locations outside the polar regions. ICESat-2 tracks are offset in the mid-latitudes to increase the spatial density of the point cloud for biomass applications. Hu et al. (2021) measured snow depth was measured with ATL08 data at few~~ 70 ~~16 points (N=16) with slopes lower than 1.5° and snowpack shallower than 0.35 m. They suggested that this product may not be suitable for rugged topography. We expect ATL06 data to be more relevant to measure snow depth in mountains considering its higher spatial resolution.~~ Enderlin et al. (2022) compared ATL06 and ATL08 elevations with reference DEMs derived from satellite photogrammetry and airborne lidar to increase the number of snow depths retrieved. ATL08 snow depth retrievals were found to be hardly reliable in mountainous terrain, in agreement with Hu et al. (2021). However, they concluded that snow depth could be measured in mountainous terrain and over a glacier with ATL06 but lacked distributed validation data to estimate the uncertainty of the retrievals. Considering the current need to measure snow depth in 75 mountains and the increasing availability of high-precision elevation datasets, these approaches seem promising. ~~However, this application is challenging since ICESat-2 was not designed to make frequent repeat measurements at the same locations outside the polar regions. ICESat-2 tracks are offset in the mid-latitudes to increase the spatial density of the point cloud for biomass applications.~~

80 Considering the current need to measure snow depth in mountains and the increasing availability of high-precision elevation datasets In this study, we assessed the uncertainty of different approaches to retrieve seasonal snow depth from the ICESat-2 ATL06 products in complex terrain. More specifically, we studied which type either snow depth can be retrieved from ICESat-2 ATL06 measurements only (snow-on and snow-off elevations) or if an additional of external DEM is required as a snow-off elevation source. To address these questions, we explored the ICESat-2 ATL06 dataset over the upper Tuolumne basin where airborne snow depth maps are frequently acquired through the Airborne Snow Observatory (ASO) program. The 85 ASO program provides 3 m resolution snow depth maps with an uncertainty of ~0.1 m (Currier et al., 2019; Mazzotti et al., 2019). The upper Tuolumne basins covered by the program are is ideal for testing new snow depth detection methods as the acquisitions are repeated every two weeks in the melt-period since 2013 in the upper Tuolumne basin. We obtained over 100,000 snow-on points between October 2018 and November 2021 from ICESat-2 ATL06 and compared them with several snow-off elevation sources, including ICESat-2 ATL06 snow-off points, an airborne lidar DEM, a satellite photogrammetry 90 DEM and a satellite InSAR DEM that is globally available (Copernicus DEM). The ~~ICESat-2 ATL06~~ snow depth retrievals were evaluated against eight airborne lidar snow depth maps from the ASO. Our objective was to assess the uncertainties of these retrievals, and not to characterize the spatial and temporal variability of the snow depth in the upper Tuolumne. The

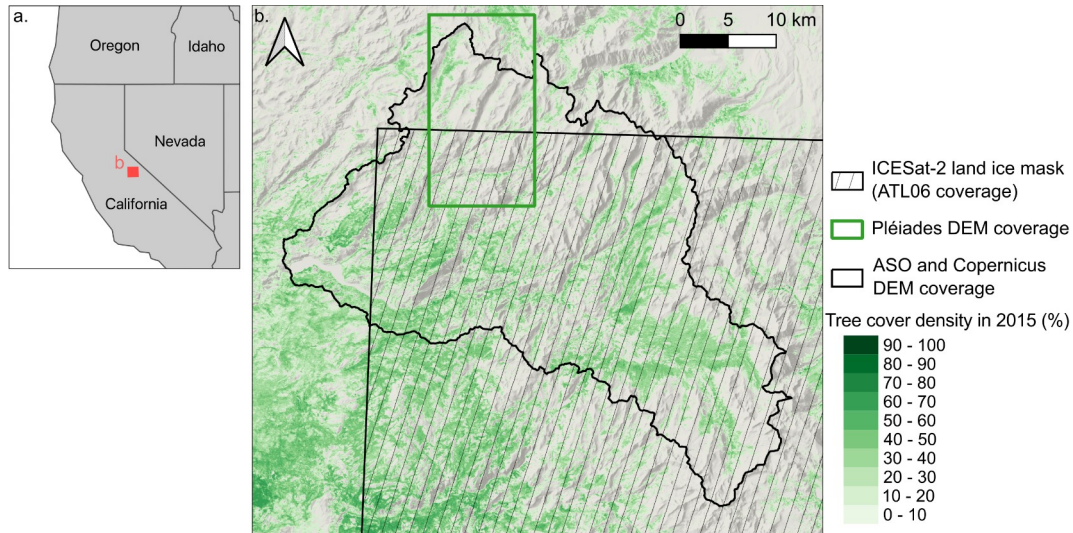
interested reader will find more information about this topic in other studies (Margulis et al., 2019; Pflug and Lundquist, 2020).

100

## **2. Study site**

The upper Tuolumne river basin is part of the Sierra Nevada mountain range (California, USA) and is contained within Yosemite National Park (Figure 1). It consists of 1100 km<sup>2</sup> of montane forests and alpine zones spanning an elevation range of 1200 m to 4200 m. Tree cover and terrain slope vary greatly within the watershed. More than half of the precipitation of this region range falls as snow (Li et al., 2017) with large year-to-year variations of snow accumulation (Pflug et al., 2022).

105



110 **Figure 1.** The upper Tuolumne basin is located in California, USA (a). The basin is entirely covered by the ASO DEM (black contour) and partially covered by the ATL06 coverage (black hatch) and by the Pléiades DEM (green rectangle). The background map shows a hillshade of the topography and the tree cover density (green shades) (b).

## 23. Materials and Methods

### 32.1 ICESat-2 ATL06 elevation product

115 ATL06 was primarily designed to provide elevation measurements on land ice, yet its coverage extends beyond glacier areas such that sparse-ATL06 data are available even in mountain ranges with very limited glacier cover such as the Sierra Nevada (Smith et al., 2019). The ATL06 product is produced-generated by fitting 40 m segments to the land-surface photon returns along each of the six tracks, with segments overlapping by 20 m. Photons returned by above ground objects (e.g. vegetation) are included. The mean surface height of each linear segment is provided as point data positioned at the center of that segment and is labeled  $h\_mean$  in the ATL06 data product (Smith et al., 2019). The height  $h\_li$  was used as it is calculated after correction of  $h\_mean$  for errors in the detection of photons by ATLAS (i.e the transmit-pulse-shape error and the first-photon-bias). The overlap of the segments results in a point located every 20 m along-track for each of the six tracks.

125 ~~The upper Tuolumne river basin spans an elevation range of 1200 m to 4200 m and consists of 1100 km<sup>2</sup> montane forests and alpine zones. All available ATL06 granulesegments resulted in 265,590 points intersecting the upper Tuolumne basin and spanning from 15 October 2018 to 7 November 2021. We excluded segments with large errors, indicated by the field  $\sigma\_h\_mean$ . Segments with errors greater than 1000 m were discarded (4% of the data). points were discarded since their elevation value was non valid (no data) as indicated by the or their error was large (field, provided with each segment.  $\sigma\_h\_mean$  We empirically excluded segments with  $\sigma\_h\_mean > 1000$  m greater than ). The number of photons used to calculate the height of each segment is provided in the field  $n\_fit\_photons$ . as snow and ice are highly~~

reflective in the ATLAS beam wavelength (532 nm). We classified snow as present when the number of photon returns exceeded a certain threshold (Figure 2 and S1). This threshold was determined by comparing the number of photons with MODIS snow cover observations. A daily stack of snow cover maps was generated by linear interpolation of the MOD10A1 “NDSI\_Snow\_Cover” in the time dimension on a pixel basis. The resulting gap-free time series of NDSI layers was binarized to snow and no-snow maps using a NDSI threshold of 0.2. Cohen’s kappa was used as the objective function to maximize to find the optimal number of photons (Cohen, 1969; Gaseoin et al., 2015). In particular, it increases over snow surfaces which are highly reflective in the ATLAS beam wavelength (532 nm). We take advantage of this property to determine the snow presence for every segment. We classified snow as present when  $n\_fit\_photons$  exceeded a certain threshold. We determined the threshold by optimizing the accuracy of the classification in comparison MODIS data. We used Terra MODIS MOD10A1 product which has a spatial resolution of approximately 500 m (Hall and Riggs 2016.). From this product, we generated a daily gap-free stack of MODIS snow cover area maps by linear interpolation of the normalized difference snow index (NDSI) in the time dimension on a pixel basis followed by a binarization to snow and no-snow using a NDSI threshold of 0.2 (Gaseoin et al. 2022). Then, we sampled the MODIS snow maps at each ATL06 segment location for the matching date. The kappa coefficient, a statistic often used to measure the consistency between two classifications (Cohen, 1969), was used to find the optimal threshold, i.e. we determined the threshold which maximized the kappa value by testing all possible values from 0 to 500 photons (Fig. S1). This optimization was done separately for the weak (N=123513) and the strong beam segments (N=132289). Figure XX shows the spatial distribution of the mean annual snow cover duration computed from the interpolated MODIS snow maps over the Tuolumne river basin.  $n\_fit\_photons$  is provided in the field  $n\_fit\_photons$ . It is used to calculate the height of each point ( $n\_fit\_photons$ ) (The number of photons

### 3.2 Snow-off elevation data

We used ~~four~~three snow-off DEMs from ~~ICESat-2 ATL06 itself~~, airborne lidar, satellite photogrammetry and satellite InSAR as explained below (Table 1):

(i) We generated the ICESat-2 snow-off DEM at 15 m resolution from all snow-off points using a gaussian weighted interpolation with a search radius of half a pixel with the point2dem utility of the Ames Stereo Pipeline (Shean et al., 2016; Beyer et al., 2018). Here, we assumed that each ATL06 point corresponds to a pixel of 15 m by 15 m.

(ii) A digital terrain model (DTM) at 3 m grid spacing was measured with airborne lidar during the ASO campaign on 13 October 2015 (Painter et al., 2016).

(iii) A DEM at 3 m grid spacing was calculated from stereographic images of the satellite Pléiades on 13 August 2017 (Deschamps-Berger et al., 2020). This DEM covers 220 km<sup>2</sup> of the upper Tuolumne basin (i.e. 20% of the total area).

(iv) A DEM was clipped from the Copernicus-30 global dataset ~~was extracted~~ at its native grid spacing of 30 m (COP-DEM-GLO-30-R, <https://doi.org/10.5270/ESA-c5d3d65>). The Copernicus-30 product was derived from InSAR data of the TanDEM-X mission in most areas, including the upper Tuolumne basin, with some areas filled with miscellaneous external products.

165 ~~The Copernicus DEM was left at its native 30 m resolution. to allow an evaluation of the true scale of ATL06 points the  
Pléiades and ASO DEMs were used at their native resolution (3 m) but also at a coarser resolution of 15 m (resampling by  
averaging the contributing pixels). this uncertainty address the exact spatial resolution of the ATL06 segments remains  
uncertain. To photons might represent the elevation at a finer scale. Thus, oflection a set the maximum sampling area of each  
ATL06 point is 40 m (i.e. the segment length) by ~11 m (i.e. the footprint width). However the extraction of the elevation at  
the center of a linear segment fitted through 06 products is different from its spacing (20 m) since the resolution of the  
ATL06 However, the exact spatial scale of the ATL06 points remains uncertain. Consistent spatial resolution between the  
170 snow-off and snow-on products is expected to improve the derived snow depth.~~

### 2.3. Vegetation and snow-cover products

175 The Terra MODIS MOD10A1 product was used to retrieve snow cover (Hall and Riggs, 2016; Figure S1). It provides daily  
snow cover maps with a spatial resolution of approximately 500 m (Hall and Riggs, 2016). The tree cover density was  
retrieved from the Landsat-MODIS product (Sexton et al., 2013) which provides the proportion of the area occupied by trees  
at 30 m resolution (Figure 1).

## 4. Methods

### 4.1. ATL06 snow-cover calculation

180 The number of photons used to calculate the height of each ATL06 segment (*n\_fit\_photons*) varies upon the land cover. In  
particular, it increases over snow surfaces which are highly reflective in the ATLAS beam wavelength (532 nm). We take  
advantage of this property to determine the snow presence for every segment. We classified snow as present when  
*n\_fit\_photons* exceeded a certain threshold. We determined the threshold by optimizing the accuracy of the classification in  
comparison to MODIS snow cover data. We first generated a daily gap-free stack of MODIS snow cover area maps by linear  
185 interpolation of the normalized difference snow index (NDSI) in the time dimension on a pixel basis followed by a  
binarization to snow and no-snow using a NDSI threshold of 0.2 (Gascoin et al. 2022). Then, we sampled the MODIS snow  
maps at each ATL06 segment location for the matching date. The kappa coefficient, a statistic often used to measure the  
consistency between two classifications (Cohen, 1969), was used to find the optimal threshold, i.e. we determined the  
threshold which maximized the kappa value by testing all possible values from 0 to 500 photons (Figure S2). This  
190 optimization was done separately for the weak (N=123513) and the strong beam segments (N=132289). Figure S1 shows the  
spatial distribution of the mean annual snow cover duration computed from the interpolated MODIS snow maps over the  
Tuolumne river basin.

### 4.2 Snow depths calculation

195 The window used to select the photons and calculate the ATL06 elevations has a maximum length of 40 m and a width  
corresponding to the ATLAS footprint that is 11 m. The ASO and Pléiades DEMs were resampled from their native

resolution of 3 m to 15 m by averaging. The 15 m resolution was selected because (i) it approximates the spatial window used to calculate each ATL06 segment and (ii) it is a multiple of the initial resolution of the source DEMs. All DEMs, ~~except the ICESat-2 snow-off DEM,~~ were co-registered to the ICESat-2 snow-off point cloud using Nuth and Kääb (2011) method.

200 This method relates the horizontal co-registration vector between two elevation datasets with the elevation difference between the two datasets, the slope and the aspect of the terrain. It can be used with gridded product (e.g. lidar or photogrammetry DEM) or irregularly distributed points (e.g. ICESat-2 ATL06). The elevation of the DEM ~~was~~ extracted at the ICESat-2 point position with a spline linear interpolation scheme (`scipy.interpolate.interp2d`). The slope and aspect ~~are~~ were calculated from the DEM and extracted with the same method. The slopes smaller than 10° and steeper than 45°  
205 (empirical thresholds) were excluded to prevent errors in the co-registration vector calculation (Nuth and Kääb, 2011). ~~The slopes steeper than 45° (i.e. prone to error in the elevation dataset) and smaller than 10° (i.e. which lead to a divergence of the Nuth and Kääb (2011) equation) are excluded.~~ A co-registration vector ~~was~~ iteratively calculated and applied to the DEM, the aspect and the slope raster. The iteration ~~was stoppeds~~ when the co-registration vector ~~wasis~~ shorter than 0.1 m or when the ~~normalized median absolute deviation~~ Normalized Median Absolute Deviation of the residual (NMAD, i.e. error  
210 metric, Höhle and Höhle, 2009) of the elevation difference ~~wasis~~ improved by less than 1%. After the horizontal co-registration vector ~~iswas~~ applied, a vertical shift ~~iswas~~ applied to the DEM based on the mode of the elevation residual distribution (Table S1).

Due to the difference in structure between the gridded snow-off DEM and the ICESat-2 snow-on points, the elevation of the snow-off DEMs ~~had to be were~~ interpolated linearly at each ICESat-2 snow-on point to calculate the “ICESat-2 derived  
215 snow depth”. ~~For the ICESat-2 snow-off DEM, the elevation was extracted at the snow-on point by nearest-neighbor interpolation as the snow-off DEM was too sparse to use a linear interpolation of neighboring pixels.~~ The ICESat-2 derived snow depth products were labeled after the snow-off DEM source ~~and resolution~~, e.g. “IS2-ASO ~~3 m~~” refers to the snow depth computed as the difference between ICESat-2 (IS2) snow-on points and ASO snow-off DEM ~~at 3 m resolution~~ (Table S2).

220



**Table 1. Elevation and snow depth dataset used in this study.**

Data	Source	Structure	<u>Snow cover</u>	<u>Spatial resolution spacing</u>	Date
Elevation points	ICESat-2 ATL06	Points	<u>Snow-on and snow-off</u>	20 m	2018-10-15 to 2021-11-07
Digital Terrain Model	Airborne lidar (ASO)	Regular grid	<u>Snow-off</u>	<u>315</u> m	2015-10-13
Digital Surface Model	Satellite photogrammetry (Pléiades)	Regular grid	<u>Snow-off</u>	<u>315</u> m	2017-08-13
Digital Surface Model	Copernicus DEM – 30 m	Regular grid	<u>Snow-off</u>	30 m	-
					2019-03-24
					2019-04-17
					2019-05-03
					2019-07-05
Snow depth map	Airborne lidar (ASO)	Regular grid	=	<u>153</u> m	2020-04-13
					2020-05-07
					2020-05-22
					2021-04-29
<u>Tree cover density</u>	<u>Landsat-MODIS</u>	<u>Regular grid</u>	=	<u>30 m</u>	<u>2015</u>
<u>Snow cover</u>	<u>MOD10A1</u>	<u>Regular grid</u>	=	<u>500 m</u>	<u>2018-10-15 to 2021-11-07</u>

#### **4.33.2 Evaluation of the snow depths**

Eight snow depth maps at 3 m grid spacing from the ASO program were available at different dates over the study period (Table 1). The maps were shifted horizontally according to the vector used to co-register the ASO DTM to the ICESat-2 snow-off points. The ASO snow depth maps ~~were used at their native resolution and~~ were also resampled by averaging at 15 m to evaluate the scale of ATL06 points. For each ICESat-2 derived snow depth, the snow depth value of the closest ASO snow depth map in time was extracted. ~~Hereafter, We used~~ the term accuracy ~~or bias to describe systematic errors to describe biases~~ in snow depth while precision ~~was~~ used for random errors (Hugonnet et al., 2022). The accuracy of the ICESat-2 derived snow depths was evaluated with the median of the residuals (e.g. IS2-ASO-~~3 m~~ snow depth minus ASO snow depth) while the precision was evaluated with the ~~NMAD~~ Normalized Median Absolute Deviation of the residual (NMAD, Höhle and Höhle, 2009), a measure of dispersion robust to outliers. ~~The ICESat-2 derived snow depth were~~

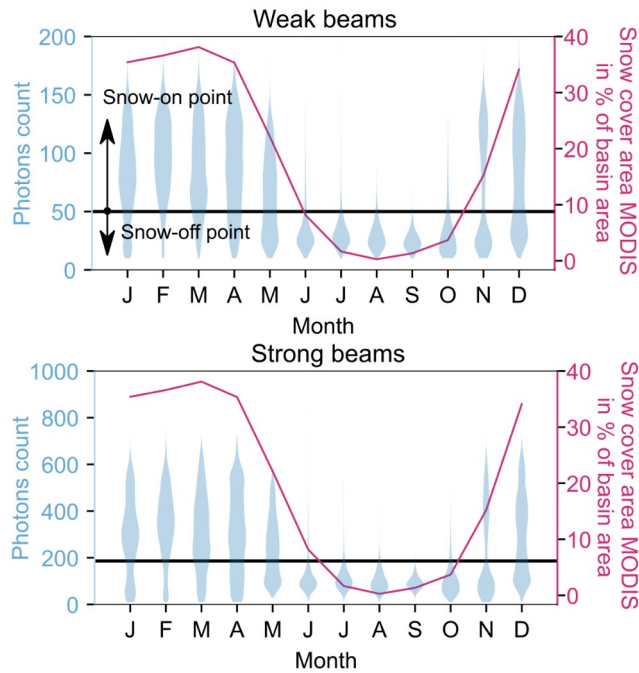
initially calculated using segments from all beams. The calculations were also repeated distinguishing strong and weak beams.

235 The uncertainty of airborne and satellite laser elevations increases when the slope increases as steep slopes spread the photons return timing compared to flat terrain (Deems et al., 2013; Treichler et al., 2017). This holds for photogrammetry derived elevation as well, due to the strong distortion of the images in the steep slopes (Berthier et al., 2007; Lacroix, 2016). Thanks to the spatially dense photon detection of ICESat-2, the uncertainty of ATL06 only increases for slopes greater than 60° (Figure S3). We evaluated the impact of slopes on ICESat-2 derived snow depth thanks to slope maps derived from the  
240 ASO DTM ~~at 3 m and 15 m~~. Vegetation (bushes, isolated trees, forests) is also expected to impact the accuracy and precision of the ICESat-2 derived snow depths as vegetation is handled differently in each elevation source (Deems et al., 2013; Smith et al., 2019; Piermattei et al., 2019). The ICESat-2 ATL06 points were produced without explicitly excluding the photons reflected by the vegetation, thus including photons from the top of the canopy to the ground. The ASO DEM is a DTM, i.e. the ground surface is measured with vegetation excluded. The Pléiades DEM measures the visible surface of the vegetation,  
245 i.e. a digital surface model. Therefore, the impact of the vegetation on the ICESat-2 derived snow depths was also evaluated using the tree cover density ~~at each point position~~ from the Landsat-MODIS 30 m product (Sexton et al., 2013).

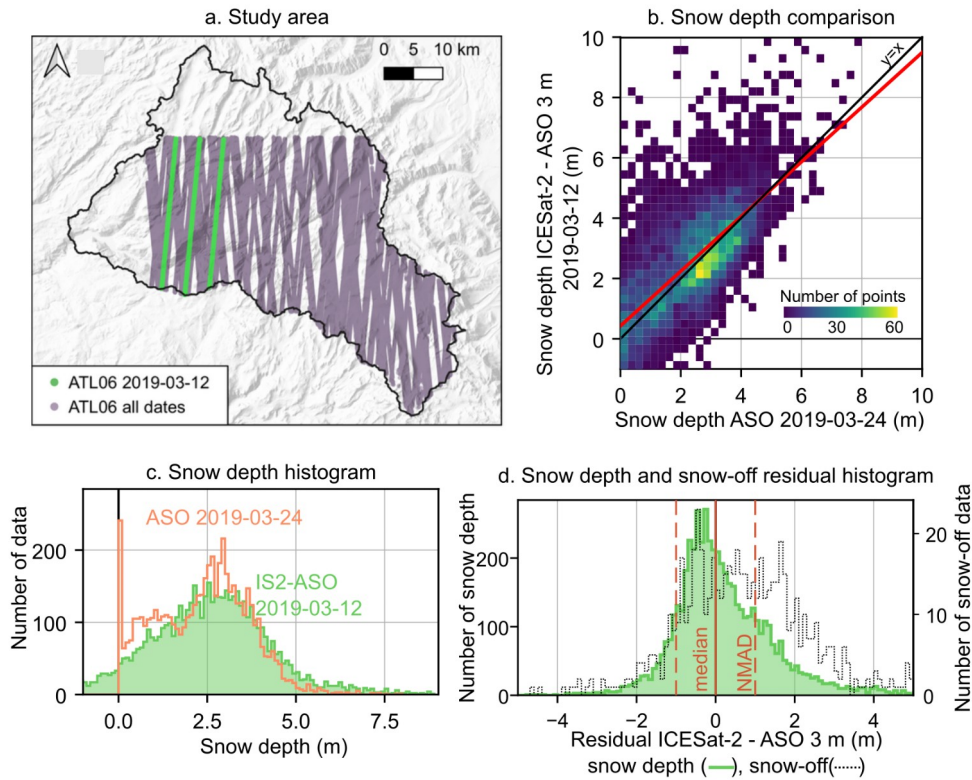
## 5 Results

### 250 5.1 Spatial and temporal data availability of ATL06

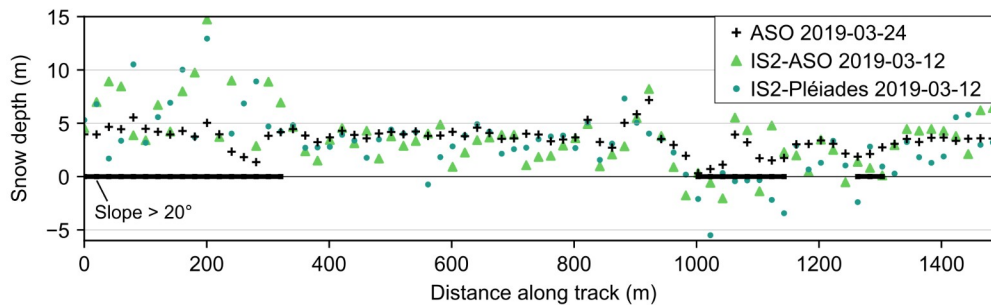
Figure 3a shows the 255,802 ATL06 points available over the 1100 km<sup>2</sup> of the upper Tuolumne river basin between 15 October 2018 and 7 November 2021. The number of photons returned for each ATL06 pointsegment varies seasonally and is lowest from June to October during the snow-free season (Figure 2). ~~The optimization of the photon count threshold is robust (Figure S1) with 50 photons for the weak beam points and 186 photons for the strong beam points~~  
255 The optimization of the photon count threshold gives a clear and unique optimum (Figure S2) with 50 photons for the weak beam points and 186 photons for the strong beam segments. With these thresholds, 59% of the points were classified as snow-off. ~~This results in a sparse ICESat-2 snow-off DEM with 25 km<sup>2</sup> of valid data on a grid of 15 m resolution, which is 2% of the basin (Figure 3), since many pixels were not intersected by an ATL06 point.~~ The remaining snow-on points were distributed on 50 dates with half of the dates containing less than 700 points and the remaining dates with more, up to 8000 points, which means at best a  
260 coverage of 1.8 km<sup>2</sup> at a single date if gridding the points on a 15 m grid ~~(Figure 1a)~~. About half of the points were in areas with a low tree cover density (< 10%) of which 45% were snow-covered. Some snow-on and snow-off points were obtained in areas with higher tree cover density up to 70%, close to the maximum observed in the upper Tuolumne basin (72%).



265 | **Figure 2.** Distribution of photons counts by beam and month for ICESat-2 ATL06 points ([blue](#)). ICESat-2 has three pairs of beams. Each beam of a pair is either strong or weak depending on the number of photons per pulse. The photon count thresholds to determine snow-on and snow-off points [were](#) optimized with MODIS snow cover [area and](#) are marked by a black line. The monthly mean snow cover area from MODIS over the period is in red. [A map of the the snow cover duration derived form the MODIS time series is provided in Figure S1.](#)



270 **Figure 3.** (a) All the ICESat-2 ATL06 points available over the upper Tuolumne basin between October 2018 and November 2021 (purple), with the 12 March 2019 track highlighted (green). Heat-map (b) and general distribution (c) of the ICESat-2-ASO snow depth on 12 March 2019 (green) and airborne lidar snow depth twelve days later (orange). Histogram of the snow depth residual (green) and the snow-off residual (black dashed) (d). Red lines show the median plus/minus the NMAD of the snow depth residual.



275 **Figure 4.** Transect of the snow depths on 12 March 2019 derived from ICESat-2 – ASO (green triangles), ICESat-2 – Pléiades (green circles) and on 24 March 2019 by the ASO (black cross). Slopes steeper than 20° are marked on the X-axis as an indication of areas prone to errors. This transect is the northernmost of the first beam available on that date (Figure 3a).

## 5.2 Impact of the snow-off DEM source

Few snow-on points intersected the ICESat-2 ATL06 snow-off DEM, due to its sparse coverage (Figure 3). The other gridded external DEMs provided over 10 times more snow depth points due to their higher incidence of overlap with ATL06 snow-on points. In the next sections we present results for 12 March 2019 as it is the only date with snow-on points covering a large range of snow depth, which intersect the Pléiades snow-off DEM coverage and with an ASO snow depth map acquired only 12 days later. The snowpack changed a little as the Lower Kibbie Ridge station (2042 m a.s.l., 10 km east of the within the basin, SNOTEL data) measured +0.01 m water equivalent (w.e.) accumulation between the ICESat-2 track (12 March) and the ASO snow depth map (24 March) (SNOTEL data).

On 12 March 2019, we obtained the best results from the combination of ICESat-2 ATL06 and ASO 3-m snow-off DEM, (IS2-ASO 3 m) and ICESat-2 ATL06 and Pléiades 3 m snow-off DEM (IS2-Pléiades 3 m) (Figure 3, 4, 5, Table S2). The ICESat-IS2-ASO derived snow depths have a low no bias of 0.0 m (median=0.00 m median IS2) and a precision of 1.00 m (NMAD) -0.17 m (median IS2-Pléiades 3 m), and a precision of 1.19 m (NMAD IS2-ASO 3 m) and 1.11 m (NMAD IS2-Pléiades 3 m). IS2-Pléiades snow depths have a similar precision (NMAD=1.08 m) but a negative bias (median=-0.53 m). More points were available for IS2-ASO 3 m (N=544950) than IS2-Pléiades 3 m (N=1295), making the evaluation more robust for the former, but also possibly impacting differently the uncertainties of each methods on that date (see 5.3 and 5.4). Negative snow depths in IS2-ASO represent 10% of the snow depths (Figure 3c). They are found over shallow snowpacks and in areas with slopes greater than 10°. The 127 snow depths available for IS2-IS2 15 m had a larger bias (median=-1.03 m) and worse precision (NMAD=3.63 m). The IS2-Copernicus 30 m snow depths showed the worst precision (NMAD=3.00 m) and a low accuracy (median=-0.53 m) and precision (NMAD=m) (Table S2). Thus, we disqualified the IS2-Copernicus 30 m snow depths and excluded them from the following analysis (Figure S4).

The other dates mirror the accuracy and precision found on 12 March 2019 for IS2-ASO (Figure 5d). The NMAD of the snow depth residuals on the eight dates available for evaluation ranges from 0.60 m to 1.16 m, 0.89 m on average. The median of the residuals ranges from -0.65 m to 0.23 m, -0.17 m on average, with the exception of The two other dates available for the evaluation of IS2-Pléiades show a similar precision with NMAD equal to 1.01 m and 1.16 m while the accuracy was lower with median residuals of -0.68 m and -0.90 m (Figure 5e). The snow-off residuals of IS2-ASO have a lower precision than the snow depths residuals with a NMAD of 1.28 m over all snow-off points (Figure S8, Table S2). The same is observed for the IS2-Pléiades residuals with an NMAD of 1.47 for all snow-off points, the precision of IS2-Pléiades 3 m which were degraded on 15 July 2019 (NMAD=1.57 m) and 10 May 2021 (NMAD=1.55 m). The median bias of IS2-ASO 3 m is smaller in absolute than 0.15 m for five dates and between -0.26 m and -0.58 m for the three other dates. On that date, the precision was better (NMAD=1.65 m) than on 12 March 2019 (NMAD=3.63 m) but the accuracy was worse (median=-0.85 m). The IS2-IS2 15 m might be better evaluated on 14 May 2019 where snow-off and snow-on tracks were nearly collocated, providing 2760 snow depth points. This is likely a result of actual snow depth change as the Lower Kibbie Ridge station measured 0.28 m w.e. ablation between the ASO snow depth map (3 May) and the IS2 track (1 May).

### 5.3 Impact of the terrain slope

ICESat-2 derived snow depth showed a general better agreement with ASO snow depth in areas with low slopes (Figure 5 a). For slopes below 10°, IS2-ASO-3 m and IS2-Pléiades-3 m had a better precision with a NMAD of, respectively, 0.39 m and 0.84 m on 12 March 2019 compared to 1.00 m and 1.08 m for all snow depths on that date. ~~The precision was worse for IS2- IS2-15 m (NMAD=1.68 m).~~ The accuracy for this range of slopes was similar-lower for IS2-ASO all-products (i.e. (median= between -0.35 m) compared to all the points available that date (median=0.00 m). ~~and The IS2-Pléiades accuracy was similar with a median of -0.563 m.~~ ~~Note that t~~ The co-registration corrected the vertical bias on all points with slopes up to 45° and cannot ensure a lack of bias for any subset of slopes (e.g. slopes between 0° and 10°).

IS2-ASO-3 m snow depths precision and accuracy worsened with increasing slope. The median residual increased gradually from -0.35 m for slopes between 0° and 10° to +0.5973 m for slopes between 30° and 40° in contrast with the median residual of IS2-Pléiades which decreased in absolute by 0.14 m only from -0.56 m to -0.42 m. Over the same range of slopes, the precision of IS2-ASO decreased as well with the NMAD growing from 0.39 m to 1.48 m. The NMAD of IS2-Pléiades-3 m grew comparatively less, from 0.84 m to 1.42 m for the same slopes.

### 5.4 Impact of the vegetation density

The IS2-ASO-3 m snow depth accuracy and precision were roughly constant up to 60% of tree cover density, i.e. the maximum sampled by the 12 March 2019 tracks (Figure 5b). This suggests that ICESat-2 ATL06 points captured the surface elevation below the canopy in this area despite the vegetation. ~~However, the distribution of the elevation difference between ICESat-2 snow-off points and ASO DTM was positively skewed (-), suggesting that vegetation partly led to an overestimation of the ground elevation for snow-off ATL06 points. Acknowledging this, we used the mode of the residual distribution to vertically co-register the ASO DTM. Using the median, i.e. as often done (Deschamps-Berger et al., 2020; Shean et al., 2020), would increase the snow depth bias by 0.54 m.~~ The IS2-Pléiades-3 m snow depth was sensitive to the tree density with a decrease in precision and a strong negative bias for tree cover density between 30% and 40% (median=-1.52 m) and between 40% and 50% (median= -4.12 m) compared to the best results measured with tree cover density lower than 10% (median= -0.20 m). The precision decreased as well from areas with low tree cover density (NMAD=0.98 m) to areas with tree cover density between 40% and 50% (2.51 m).

### 5.5 Scale of the ICESat-2 ATL06 measurements and iImpact of the beam strengths and of the elevation retrieval algorithm

Considering separately the snow-on points of the strong or the weak beam yield lower precision and larger biases for the strong beam on 12 March 2019 for IS2-ASO and IS2-Pléiades (Figure S5 and S6 a to c). The bias of IS2-ASO from the weak beam are smaller than the one from the strong beam at most dates but the impact of the beams strength on the precision is not systematic at all dates (Figure S5 and S6 d and e).

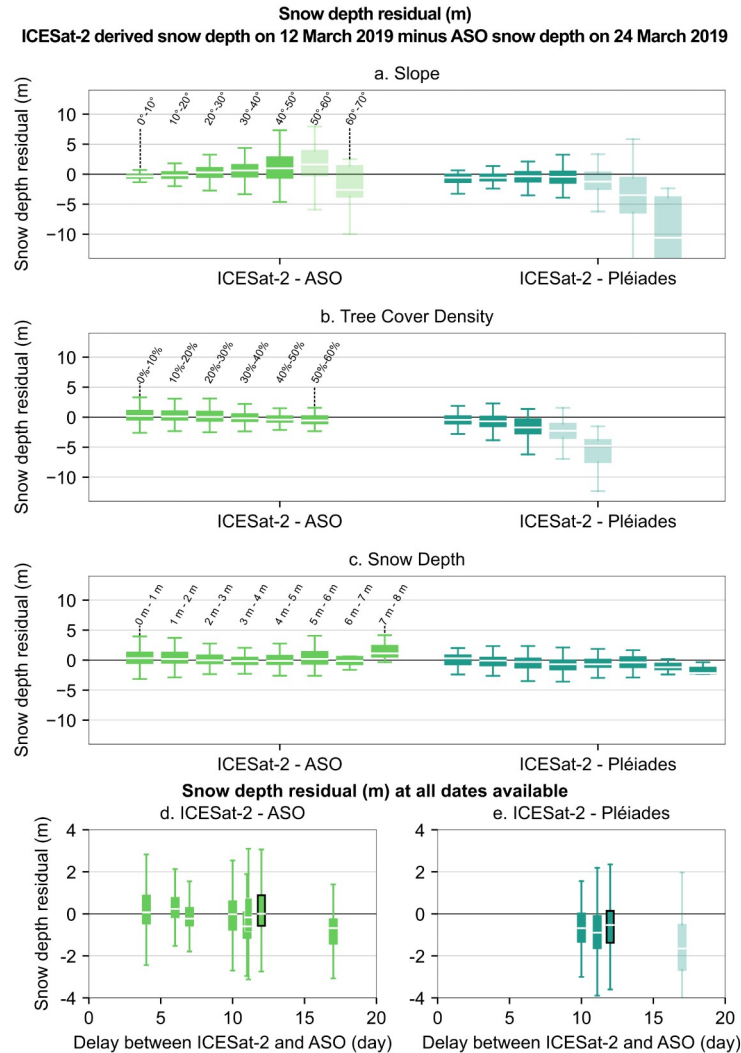


**Figure 5.** Snow depth residuals (ICESat-2 derived snow depth minus ASO snow depth). Each group of boxplots (or color) corresponds to a snow-off DEM. Within each group, the boxplots are classified by terrain slope (a, b), tree cover density (b, c, d) and snow depth (c, e, f). The residuals were calculated from the product at their native resolution (a, c, e) or averaged at 15 m for ASO-DEM, Pléiades-DEM and ASO snow depth (b, d, f). The snow depth derived from ICESat-2 and the ASO 3-m-DEM are the most accurate and precise for all tree cover densities. DEM have a similar precision for open or flat terrain but a better for steeper slopes. 3 m The snow depth retrieved from ICESat-2 and Pléiades Snow depth residuals when an ASO snow depth map is available at less than 20 days (d, e, g, h, i). Transparent

boxplots show the dataes where less than 100 points were available. The black boxplot is the residual on 12 March 2019 shown in upper panels. ~~Higher temporal resolution and more points per date are available using gridded DEMs with full coverage of the study area (g, h). The best precision and accuracy is obtained with the ASO DEM (g) and the Pléiades DEM (h). The sampling of the~~  
breakdown variables differs due to the different coverage of the snow-off DEMs.

## 6.4 Discussion

The snow depth retrieved from ICESat-2 ATL06 data only (IS2-IS2 15 m) might not prove useful to many applications in terms of temporal and spatial availability. The ICESat-2 snow-free DEM coverage is currently sparse, but is expected to improve over time as new tracks are acquired by the satellite at these latitudes. The retrieval of the IS2-IS2 15 m snow depth through nearest-neighbor interpolation is suboptimal as it does not take into account the variation of the terrain. Better results are expected if a linear or cubic interpolation at the intersection between the snow-off and the snow-on track is conducted.

Using an external DEM as a snow-off reference improves the data coverage and allows the use of every ICESat-2 snow-on point.

### 6.1. Impact of the snow-off source

The most accurate and precise snow depths best results were obtained with the airborne lidar DTEM\_ ~~and the satellite photogrammetry DEM (e.g. IS2-ASO, IS2-Pléiades 3 m 3 m). The airborne lidar DTM measures the ground surface below the tree canopy and ensures ICESat-2 snow depth retrieval even in forest with density up to 60%. The bias measured were typically 0.20 m in absolute and the precision around 1.20 m or less. The errors in snow depth increase with slope but do not depend on the tree cover density. The airborne lidar DTM measures the ground surface below the tree canopy and ensures ICESat-2 snow depth retrieval even in forest with density up to 60%, close to the maximum observed in this area. Airborne lidar datasets are increasingly freely available in parts of the world (e.g. in Northern America and Europe). Yet, the vast majority of the world's mountains remain uncharted.~~ Our results suggest that using a satellite photogrammetry snow-off DEM (e.g. IS2-Pléiades) is a viable alternative in some areas as it provides snow depth with a similar accuracy and precision to airborne lidar for tree cover density below 320% and low slopes ~~estimation of snow depth in steep slopes better and even a~~. The satellite photogrammetry DEM includes vegetation which degrades rapidly the derived snow depth when the tree cover density increases and leads to marked bias. The lidar airborne and satellite snow depth uncertainties differ largely in slopes with the increase of the bias for IS2-ASO with slope compared to the constant bias for IS2-Pléiades (Figure 5a). This discrepancy between the two DEMs is observed as well even when they are co-registered together (Figure S2 in Deschamps-Berger et al., 2020) but remains unexplained. No trend in the snow depth residual with the delay between ICESat-2 and ASO acquisition date was detected (Figure 5 d, e).

The advantage of combining ICESat-2 with external DEMs to retrieve snow depths compared to times series of DEMs, is that the former method only requires a single DEM to then retrieve snow depth for all further ICESat-2 data which are freely available. On the contrary, the acquisition of a time series of DEMs requires costly and repeated airborne campaigns (Painter et al., 2016) or satellite tasking (Deschamps-Berger et al., 2022). Airborne lidar datasets are increasingly freely available in



parts of the world (e.g. in Northern America and Europe). Yet, the vast majority of the world's mountains remain uncharted. High-resolution DEMs from satellite photogrammetry are already available in the Arctic (Porter et al., 2018), the Antarctic (Howat et al., 2019) and the Himalayas (Shean, 2017). However, the time stamp is not provided in the mosaiced products and this might hinder the identification of the snow-off from the snow-on pixels. In other areas, images from the Pléiades, WorldView or the Planet-SkySat satellites can be acquired on-demand to generate a snow-off DEM. The Copernicus-30 DEM has a global coverage but its ~~uncertainties coarse-resolution\_ seems to be disqualifying for this application. partly because it hampers an accurate co-registration.~~

~~The residual elevation difference between both DEMs is close to 0 m on low slope and increases up to ~1 m for steeper slopes (Figure S2 b). This matches the comparison of the two DEMs when they are co-registered together (Figure S2 in Deschamps-Berger et al., 2020). The co-registration is considered successful for the ASO snow-off DEM and the Pléiades DEM considering the decrease of the error metric over the stable terrain (Table S1). However, the precision of the IS2-Copernicus 30 m snow depths was improved when the Copernicus DEM was co-registered to the ASO DEM (NMAD=7.03 m) rather than to the ICESat-2 snow-off points (NMAD=10.92 m) (Figure S2 and S3). This approach could not be applied in the general case as an accurate airborne lidar DEM is needed. The Copernicus 10 m product might have sufficient accuracy to derive snow depth but is only available over Europe.~~

ATL06 snow-off segments might be used as snow-off elevation reference. This would prevent mixing various sources of dataset and allow relying solely on free, open access data. However, in the three years of the study period, only 2% (25 km<sup>2</sup>) of this mid-latitude basin were observed without snow (Figure S11). Assuming the 8.2 km<sup>2</sup> y<sup>-1</sup> coverage rate remains steady, more than 50 years will be needed to cover half of the basin. Besides, this rate might decrease in the future as more and more ATL06 segments will be redundant and the proportion of areas seasonally snow-covered to be mapped will increase. Thus, we do not foresee the possibility to map snow depth out of the polar regions with ICESat-2 data only. At best, it might be possible to retrieve snow depth at a few points using a method of interpolation at the crossing points of tracks (Moholdt et al., 2010). More overlapping segments should be available in the Arctic and Antarctica thanks to the repeated orbits in the polar regions.

## **6.2 Application of the methods to other sites**

The approach described in this article should be transferable in other mountain basins, provided a high-resolution DEM is available. The classification of the segment snow cover and the co-registration approach might have to be adapted in future studies.

We used the photon counts variable provided with ATL06 segments to determine the snow cover of each segment. It remains uncertain whether the thresholds found here could be transferred in regions with different vegetation cover, terrain roughness and cloudiness, all of which affect the number of returned photons. In addition, the optimal thresholds for a given region might vary seasonally due to the evolution of the snow albedo and to the vegetation phenology. Further development of this

420 approach could benefit from using higher resolution snow cover maps derived from Sentinel-2 or Landsat images to refine the thresholds or evaluate the snow cover uncertainties (Gascoin et al., 2019).

The horizontal co-registration of the ASO and Copernicus DEMs were small and did not significantly improve the NMAD over the snow-off terrain (Table S1). In contrast, the Pléiades DEM was shifted by 5.63 m by the co-registration which improved the NMAD by 25%. We co-registered the Copernicus DEM and the Pléiades DEM to the ASO DEM after co-  
425 registration to the ATL06 snow-off points to evaluate the success of the co-registration processes (Table S3). The small residual shift, with respect to the DEMs resolution, of 0.70 m and 1.38 m respectively for the Pléiades and the Copernicus DEM highlights the good relative agreement of the co-registration. The vertical co-registration were significant with 1.15 m for Pléiades DEM and -0.65 m for the Copernicus DEM and could lead, if applied, to changes in the accuracy of the snow depths. It seems preferable to co-register the snow-off DEM to the ICESat-2 data as these biases are specific to the elevation  
430 sources, in relation with differences in the vegetation measurements and to the slope-related bias (Figure 5a). The distribution of the elevation difference between ICESat-2 snow-off points and ASO DTM was positively skewed (Figure S8), suggesting that vegetation partly led to an overestimation of the ground elevation for snow-off ATL06 points. Acknowledging this, we used the mode of the residual distribution to vertically co-register the ASO DTM. Using the median (Deschamps-Berger et al., 2020; Shean et al., 2020), would increase the snow depth bias by 0.56 m. The possibility to  
435 calculate a single co-registration vector per DEM might depend on the scale of the study site. Here, we were able to successfully map snow depth in areas of 900 km<sup>2</sup> (intersection of the ASO DEM and ATL06) and 70 km<sup>2</sup> (intersection of the Pléiades DEM and ATL06). Refined co-registration of tiles covering each a quarter of the ASO DEM did not lead to substantial improvement (not shown here). Co-registration of individual ATL06 transect with airborne lidar or satellite photogrammetry DEM in Alaska (USA) and Idaho (USA) yielded horizontal shift in various directions, up to 2.9 m, with no  
440 overall systematic shift (Enderlin et al., 2022). The co-registration of individual tracks in the upper Tuolumne basin would be practically impossible at some dates due to the lack of snow-off terrain.

### 6.3 Comparison to existing studies

The snow depths derived here from ICESat-2 ATL06 are more accurate, have a finer spatial scale and a denser spatial  
445 coverage than snow depths derived with a similar approach from ICESat products (Treichler and Kääb, 2017). ICESat derived snow depths had an RMSE of 1 m over slopes lower than 10° at the 70 m footprint scale (N=27) and steeper slopes were excluded as prone to large errors in ICESat. Here, ~~we obtained the IS2-ASO snow depths~~ have an RMSE of 0.85 m (N=907) over slopes lower than 10° on 12 March 2019 at a 3 m scale (~~IS2-ASO 3 m~~). The progressive degradation of the accuracy with the increasing slope was also characterized and found to be less pronounced for IS2-Pléiades ~~3 m~~ than IS2-  
450 ASO ~~3 m~~. The rough and vegetated mountain terrain of our study site, as expected, degrades ATL06 accuracy. ATL06 elevations were ten times more accurate over the Antarctic ice sheet than the elevation difference evaluated in this study with a precision of 0.09 m (standard deviation) compared to GNSS measurements (Brunet et al., 2019). The calculation of ATL06 elevation from ATL03 products was optimized for glaciers and ice sheets which often have flat ~~and~~ smooth and highly

455 | reflective surfaces. Improved precision might be obtained by adapting this processing to mountainous terrain (Shean et al., 2022).

The ICESat-2 ATL06 snow depths (NMAD between 0.5 m and 1.2 m) awere less precise than snow depths derived from airborne lidar only (Mazzotti et al., 2019) and similar or slightly worse than what itwas obtained with satellite photogrammetry only (Eberhard et al., 2021, Deschamps-Berger et al., 2020). In terms of relative error, the snow depth shows a typical error of 40% or less for snow depth thicker than 2 m and larger errors for shallower snowpack (Figure S7).  
460 This is comparable to the error of snow depth retrieved from Sentinel-1 (Lievens et al., 2022). Thus, the existing approaches combining satellite photogrammetry or Sentinel-1 snow depth with snowpack models (e.g. assimilation) should be appropriate for ICESat-2 derived snow depth (Shaw et al., 2020, Deschamps-Berger et al., 2022, Alfieri et al., 2022). However, ICESat-2's variable temporal resolution and sparse transect data is unique compared to spatially continuous airborne or satellite maps and gridded snow model results. Figure 6S shows the inter-annual variability of the snow depth  
465 gradient with elevation measured by the ICESat-2 track. The ICESat-2 track only covers parts of the elevation with snow cover, and the snow depth distribution sometimes differs in both datasets over the sampled altitudes. Only relying on sparse ICESat-2 derived snow depths would lead to an inaccurate estimation of the snow volume of the basin. One Estimation of the snow volume in a basin from ICESat-2 data requires to overcome the spatially discontinuous and variable sampling of ICESat-2 for instance through extrapolation based on topographical variables (Molotch et al., 2005, McGrath et al., 2018) or  
470 through data assimilation (Magnusson et al., 2014, Cluzet et al., 2022). Another promising approach to utilizing ICESat-2-derived snow depth transects comes from Pflug and Lundquist (2020), where snow patterns in the upper Tuolumne basin were shown to be repeating and scalable. Small strips of snow depths were matched with a library of distributed snow depth maps from prior years to produce distributed snow depth maps of the basin. An ICESat-2 track might be used in this way to represent a relevant subset of a basin.

475 | Each ICESat-2 ATL06 snow depth point is informative over a small sampling area as the snow depth seems as representative of 3 m pixels as of 15 m pixels (Figure ). The good quality of snow depth derived from ATL06 at this fine scale suggests that ATL03 products might provide finer scale and spatially richer snow depth, as each photon returned to ICESat-2 is provided in this product.

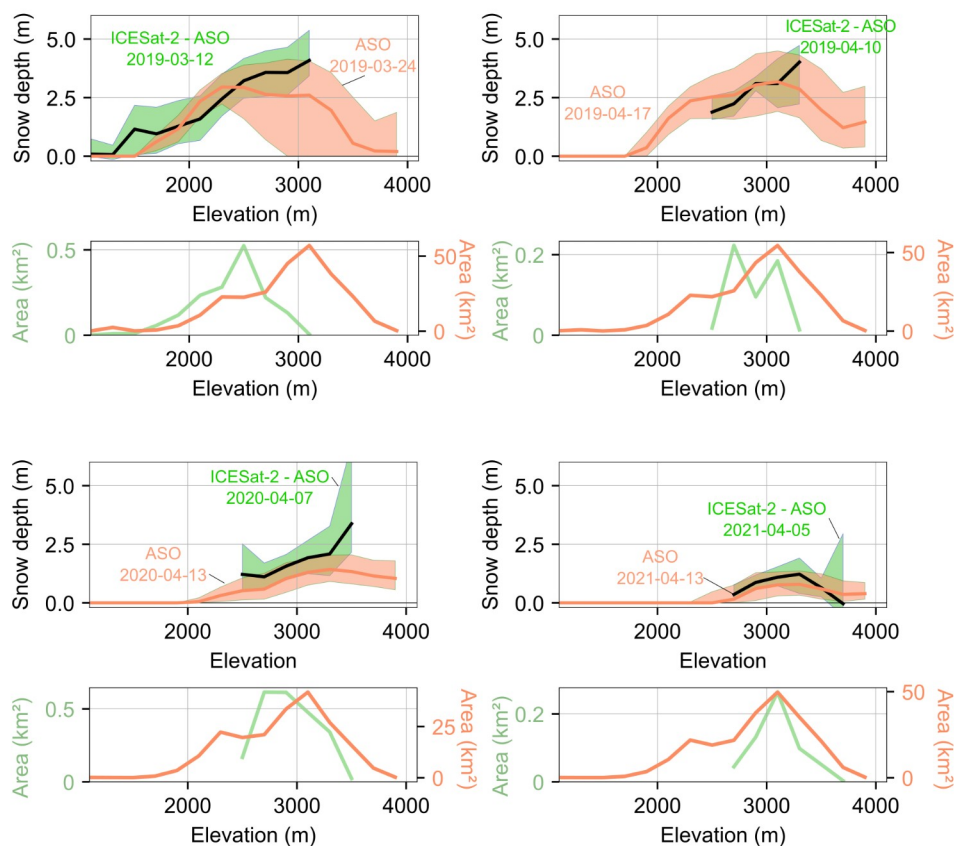


**Figure 6.** Snow depth gradient with elevation (top) from ICESat-2 and ASO snow-off (green) on four selected dates over the three winters of the period and from the closest in time ASO snow depth map (orange). Hypsometry of the snow covered areas is shown below. The y-axis scale of bottom plots differs to increase the visibility of the smaller surfaces sampled by ICESat-2.

## 76 Conclusion

The retrieval of snow depth from ICESat-2 ATL06 data only is currently limited by the coverage of the ATL06 snow-off points, but the point density will increase as long as the ICESat-2 mission continues. However, ICESat-2 ATL06 snow-on elevation combined with airborne lidar or satellite photogrammetry snow-off DEMs is a promising way to measure accurate snow depth at high-resolution in mountains. We found that little filtering of the ATL06 points was required and that a single co-registration of the snow-off DEM was sufficient. The photon counts variable provided with ATL06 pointssegments can be used to classify snow-on and snow-off points. It remains uncertain whether the threshold found here could be transferred in regions with different vegetation cover, terrain roughness and cloudiness. By combining ICESat-2 snow-on pointssegments with an airborne lidar or satellite photogrammetry DEM, a precision of ~1.2 m and a bias of ~0.2 m was obtained for a typical mountain environment, i.e. which includes snow depths up to 8 m and a large range of slope. More

precise snow depth were measured over low slopes (~0.5 m). Similar precision and bias were found for snow depth derived from ICESat-2 and a satellite photogrammetry DEM over low slopes and in terrain with low tree cover density. As expected, increasing slope degrades the snow depth retrieval while ~~+~~However, a dense tree cover mostly degraded the snow depth derived from ICESat-2 products ~~ATL06 combined with and~~ a digital surface model (i.e. satellite photogrammetry) but had little impact if ATL06 was combined with a digital terrain model (e.g. from airborne lidar). The good quality of the snow depths derived from ATL06 suggests that ATL03 products might provide finer scale and spatially richer snow depth, as each photon returned to ICESat-2 is provided in this product. ICESat-2 ATL06 derived snow depths are a valuable source of information which should be combined with modeling to inform on the amount of water stored in mountains basins and characterize its spatial and temporal variability. Given the promising results reported here, we believe that the generation of ATL06 products over non-glacierized mountainous regions is desirable to help with water resources estimation in unmonitored mountains.

### Author contribution

CDB and SG designed the study. AG performed the initial data curation under and formal analysis further led by CDB and SG. DS and HB contributed to the methodology and the validation of the results. All authors contributed to writing the manuscript. SG and JNL ensured the funding acquisition.

The authors declare that they have no conflict of interest.

### Acknowledgments

The authors thank D. Treichler and two anonymous reviewers for their constructive comments. This work has been supported by the Programme National de Télédétection Spatiale (PNTS; grant no. PNTS-2018-4), the Centre National d'Études Spatiales (CNES) and by the Spanish Ministry of Science and Innovation (MARGISNOW project, PID2021-124220OB-100). SG is supported by CNES. AG was supported by Météo-France during the internship which laid the groundwork of this article. We thank Etienne Berthier for reading an advanced version of the manuscript and providing helpful suggestions.

### Open Research

ICESat-2 ATL06 data were downloaded from <https://nsidc.org/data/ATL06/versions/5> on 1 March 2022

ASO snow depth maps and digital surface model were downloaded from [https://nsidc.org/data/ASO\\_3M\\_SD/versions/1](https://nsidc.org/data/ASO_3M_SD/versions/1) and <https://data.airbornesnowobservatories.com/#>

The Pléiades DEM is available at <https://zenodo.org/record/6466891#.Y10SuNPP02w>

Copernicus 30 m DEM was downloaded from <https://spacedata.copernicus.eu/web/cscda/data-access>

Code is available at <https://framagit.org/cesaradb/icesat-2-mapping-of-snow-height.git>

## References

- Alfieri, L., Avanzi, F., Delogu, F., Gabellani, S., Bruno, G., Campo, L., Libertino, A., Massari, C., Trapanelli, A., Rains, D.,  
530 Miralles, D. G., Quast, R., Vreugdenhil, M., Wu, H., and Brocca, L.: High resolution satellite products improve hydrological modeling in northern Italy, *Hydrology and Earth System Sciences Discussions*, December, 1–29, [doi.org/10.5194/hess-26-3921-2022](https://doi.org/10.5194/hess-26-3921-2022), 2022†.
- Barnett, T. P., Adam, J. C., and Lettenmaier, D. P.: Potential impacts of a warming climate on water availability in snow-dominated regions, *Nature*, 438(7066):303–309, [doi.org/10.1038/nature04141](https://doi.org/10.1038/nature04141), 2005.
- 535 [Berthier, E., Arnaud, Y., Kumar, R., Ahmad, S., Wagnon, P., and Chevallier, P.: Remote sensing estimates of glacier mass balances in the Himachal Pradesh \(Western Himalaya, India\). \*Remote Sensing of Environment\*, 108\(3\), 327–338. <https://doi.org/10.1016/j.rse.2006.11.017>, 2007.](https://doi.org/10.1016/j.rse.2006.11.017)
- Beyer, R. A., Alexandrov, O., and Scott, M.: The Ames Stereo Pipeline: NASA’s Open Source Software for Deriving and Processing Terrain Data Special Section, *Earth and Space Science*, 5:537–548, [doi.org/10.1029/2018EA000409](https://doi.org/10.1029/2018EA000409), 2018.
- 540 Brauchli, T., Trujillo, E., Huwald, H., and Lehning, M.: Influence of Slope-Scale Snowmelt on Catchment Response Simulated With the Alpine3D Model, *Water Resources Research*, 1–17, [doi.org/10.1002/2017WR021278](https://doi.org/10.1002/2017WR021278), 2017.
- Cohen, J.: A coefficient of agreement for nominal scales, *Educ. Psychol. Meas.*, 20, 37–46, 1960.
- Currier, W. R., Pflug, J., Mazzotti, G., Jonas, T., Deems, J. S., Bormann, K. J., Painter, T. H., Hiemstra, C. A., Gelvin, A., Uhlmann, Z., Spaete, L., Glenn, N. F., and Lundquist, J. D.: Comparing Aerial Lidar Observations With Terrestrial Lidar  
545 and Snow-Probe Transects From NASA’s 2017 SnowEx Campaign, *Water Resources Research*, 55(7), 6285–6294. [doi.org/10.1029/2018WR024533](https://doi.org/10.1029/2018WR024533), 2019.
- Deems, J. S., Painter, T. H., and Finnegan, D. C. (2013). Lidar measurement of snow depth : a review. *Journal of Glaciology*, 59(215):467–479, [doi.org/10.3189/2013JoG12J154](https://doi.org/10.3189/2013JoG12J154), 2013.
- Deschamps-Berger, C., Cluzet, B., Dumont, M., Lafaysse, M., Berthier, E., Fanise, P., and Gascoin, S.: Improving the spatial  
550 distribution of snow cover simulations by assimilation of satellite stereoscopic imagery, *Water Resources Research*, 58(3), [doi.org/10.1029/2021WR030271](https://doi.org/10.1029/2021WR030271), 2022.
- Deschamps-Berger, C., Gascoin, S., Berthier, E., Deems, J., Gutmann, E., Dehecq, E., Shean, D., and Dumont, M.: Snow depth mapping from stereo satellite imagery in mountainous terrain: evaluation using airborne lidar data. *The Cryosphere*, (February):1–28, [doi.org/10.5194/tc-14-2925-2020](https://doi.org/10.5194/tc-14-2925-2020), 2020.
- 555 Dozier, J., Bair, E. H., and Davis, R. E.: Estimating the spatial distribution of snow water equivalent in the world’s mountains, *Wiley Interdisciplinary Reviews: Water*, 3(3), 461–474. [doi.org/10.1002/wat2.1140](https://doi.org/10.1002/wat2.1140), 2016.
- Eberhard, L. A., Sirguey, P., Miller, A., Marty, M., Schindler, K., Stoffel, A., and Bühler, Y.: Intercomparison of photogrammetric platforms for spatially continuous snow depth mapping, *The Cryosphere*, 15, 69–94, [doi.org/10.5194/tc-15-69-2021](https://doi.org/10.5194/tc-15-69-2021), 2021.

- 560 Freudiger, D., Kohn, I., Seibert, J., Stahl, K., and Weiler, M.: Snow redistribution for the hydrological modeling of alpine catchments, *Wiley Interdisciplinary Reviews: Water*, pages 1–16, [doi.org/10.1002/wat2.1232](https://doi.org/10.1002/wat2.1232), 2017.
- Gascoin, S., Hagolle, O., Huc, M., Jarlan, L., Dejoux, J. F., Szczypka, C., Marti, R., and Sánchez, R.: A snow cover climatology for the Pyrenees from MODIS snow products, *Hydrology and Earth System Sciences*, 19(5), 2337–2351, [doi.org/10.5194/hess-19-2337-2015](https://doi.org/10.5194/hess-19-2337-2015), 2015.
- 565 Hedrick, A., Marks, D., Havens, S., Robertson, M., Johnson, M., Micah, S., Marshall, H.-P., Kormos, P. R., Bormann, K. J., and Painter, T. H.: Direct Insertion of NASA Airborne Snow Observatory Derived Snow Depth Time Series Into the iSnoBal Energy Balance Snow Model, *Water Resources Research*, 54:8045–8063, [doi.org/10.1029/2018WR023190](https://doi.org/10.1029/2018WR023190), 2018.
- Höhle, J. and Höhle, M.: Accuracy assessment of digital elevation models by means of robust statistical methods, *ISPRS Journal of Photogrammetry and Remote Sensing*, 64(4):398–406, [doi.org/10.1016/j.isprsjprs.2009.02.003](https://doi.org/10.1016/j.isprsjprs.2009.02.003), 2009.
- 570 Howat, I. M., Porter, C., Smith, B. E., Noh, M.-J., and Morin, P.: The Reference Elevation Model of Antarctica, *The Cryosphere*, 13, 665–674, [doi.org/10.5194/tc-13-665-2019](https://doi.org/10.5194/tc-13-665-2019), 2019.
- Hu, X., Hao, X., Wang, J., Huang, G., Li, H., and Yang, Q.: Can the Depth of Seasonal Snow be Estimated from ICESat-2 Products: A Case Investigation in Altay, Northwest China, *IEEE Geoscience and Remote Sensing Letters*, 19:1–5, [doi.org/10.1109/LGRS.2021.3078805](https://doi.org/10.1109/LGRS.2021.3078805), 2021.
- 575 Hugonnet, R., Brun, F., Berthier, E., Dehecq, A., Mannerfelt, S., Eckert, N., Farinotti, D.: Uncertainty analysis of digital elevation models by spatial inference from stable terrain, *IEEE Journal of Selected Topics in Applied Earth Observations and Remote Sensing*, 1–17, [doi.org/10.1109/JSTARS.2022.3188922](https://doi.org/10.1109/JSTARS.2022.3188922), 2022.
- [Lacroix, P.: Landslides triggered by the Gorkha earthquake in the Langtang valley, volumes and initiation processes. Earth, Planets and Space, 68\(1\), 46. https://doi.org/10.1186/s40623-016-0423-3, 2016.](https://doi.org/10.1186/s40623-016-0423-3)
- 580 Lievens, H., Brangers, I., Marshall, H. P., Jonas, T., Olefs, M., and De Lannoy, G.: Sentinel-1 snow depth retrieval at sub-kilometer resolution over the European Alps, *The Cryosphere*, 16(1):159–177, [doi.org/10.5194/tc-16-159-2022](https://doi.org/10.5194/tc-16-159-2022), 2022.
- Lievens, H., Demuzere, M., Marshall, H. P., Reichle, R. H., Brucker, L., Brangers, I., Rosnay, P. D., Dumont, M., Giroto, M., Immerzeel, W. W., Jonas, T., Kim, E. J., Koch, I., Marty, C., Saloranta, T., Schöber, J., and De Lannoy, G. J. M.: Snow depth variability in the Northern Hemisphere mountains observed from space, *Nature Communications*, 1–12, [doi.org/10.1038/s41467-019-12566-y](https://doi.org/10.1038/s41467-019-12566-y), 2019.
- 585 Magruder, L., Brunt, K., Neumann, T., Klotz, B., and Alonzo, M.: Passive Ground-Based Optical Techniques for Monitoring the On-Orbit ICESat-2 Altimeter Geolocation and Footprint Diameter, *Earth and Space Science*, 8(10):1–9, [doi.org/10.1029/2020EA001414](https://doi.org/10.1029/2020EA001414), 2021.
- Margulis, S. A., Fang, Y., Li, D., Lettenmaier, D. P., and Andreadis, K.: The utility of infrequent snow depth images for deriving continuous space-time estimates of seasonal snow water equivalent, *Geophysical Research Letters*, 46, [doi.org/10.1029/2019GL082507](https://doi.org/10.1029/2019GL082507), 2019.

Markus, T., Neumann, T., Martino, A., Abdalati, W., Brunt, K., Csatho, B., Farrell, S., Fricker, H., Gardner, A., Harding, D., Jasinski, M., Kwok, R., Magruder, L., Lubin, D., Luthcke, S., Morison, J., Nelson, R., Neuenschwander, A., Palm, S., Popescu, S., Shum, C. K., Schutz, B. E., Smith, B., Yang, Y., and Zwally, J.: The Ice, Cloud, and land Elevation Satellite-2 (ICESat-2): Science requirements, concept, and implementation, *Remote Sensing of Environment*, 190:260–273, [doi.org/10.1016/j.rse.2016.12.029](https://doi.org/10.1016/j.rse.2016.12.029), 2017.

Marti, R., Gascoin, S., Berthier, E., De Pinel, M., Houet, T., and Laffly, D.: Mapping snow depth in open alpine terrain from stereo satellite imagery, *The Cryosphere*, 10(4):1361–1380, [doi.org/10.5194/tc-10-1361-2016](https://doi.org/10.5194/tc-10-1361-2016), 2016.

Mazzotti, G., Currier, W. R., Deems, J. S., Pflug, J. M., Lundquist, J. D., and Jonas, T.: Revisiting Snow Cover Variability and Canopy Structure Within Forest Stands: Insights From Airborne Lidar Data, *Water Resources Research*, 55(7), 6198–6216, [doi.org/10.1029/2019WR024898](https://doi.org/10.1029/2019WR024898), 2019.

McGrath, D., Webb, R., Shean, D., Bonnell, R., and Marshall, H. P.: Spatially Extensive Ground-Penetrating Radar Snow Depth Observations During NASA’s 2017 SnowEx Campaign : Comparison With In Situ , Airborne , and Satellite Observations *Water Resources Research*. *Water Resources Research*, 10, [doi.org/10.1029/2019WR024907](https://doi.org/10.1029/2019WR024907), 2019.

605 National Academies of Sciences, Engineering, and Medicine: Thriving on Our Changing Planet: A Decadal Strategy for Earth Observation from Space. Washington, DC: The National Academies Press. Appendix C., [doi.org/10.17226/24938](https://doi.org/10.17226/24938), 2018.

[Moholdt, G., Nuth, C., Hagen, J. O., and Kohler, J.: Recent elevation changes of Svalbard glaciers derived from ICESat laser altimetry. \*Remote Sensing of Environment\*, 114\(11\), 2756–2767. <https://doi.org/10.1016/j.rse.2010.06.008>, 2010.](https://doi.org/10.1016/j.rse.2010.06.008)

610 Painter, T. H., Berisford, D. F., Boardman, J. W., Bormann, K. J., Deems, J. S., Gehrke, F., Hedrick, A., Joyce, M., Laidlaw, R., Marks, D., Mattmann, C., McGurk, B., Ramirez, P., Richardson, M., Skiles, S. M. K., Seidel, F. C., and Winstral, A.: The Airborne Snow Observatory: Fusion of scanning lidar, imaging spectrometer, and physically-based modeling for mapping snow water equivalent and snow albedo, *Remote Sensing of Environment*, 184:139–152, [doi.org/10.1016/j.rse.2016.06.018](https://doi.org/10.1016/j.rse.2016.06.018), 2016.

615 Pflug, J. M. and Lundquist, J. D.: Inferring Distributed Snow Depth by Leveraging Snow Pattern Repeatability: Investigation Using 47 Lidar Observations in the Tuolumne Watershed, Sierra Nevada, California, *Water Resources Research*, 56, [doi.org/10.1029/2020WR027243](https://doi.org/10.1029/2020WR027243), 2020.

620 [Pflug, J. M., Margulis, S. A., and Lundquist, J. D.: Inferring watershed-scale mean snowfall magnitude and distribution using multidecadal snow reanalysis patterns and snow pillow observations. \*Hydrological Processes\*, 36\(6\), 1–20. <https://doi.org/10.1002/hyp.14581>, 2022.](https://doi.org/10.1002/hyp.14581)

[Piermattei, L., Marty, M., Ginzler, C., Pöchtrager, M., Karel, W., Ressler, C., Pfeifer, N., and Hollaus, M.: Pléiades satellite images for deriving forest metrics in the Alpine region. \*International Journal of Applied Earth Observation and Geoinformation\*, 80\(May\), 240–256. <https://doi.org/10.1016/j.jag.2019.04.008>, 2019.](https://doi.org/10.1016/j.jag.2019.04.008)



- Porter, C., Morin, P., Howat, I., Noh, M.-J., Bates, B., Peterman, K., Keeseey, S., Schlenk, M., Gardiner, J., Tomko, K., Willis, M., Kelleher, C., Cloutier, M., Husby, E., Foga, S., Nakamura, H., Platson, M., Wethington, M., Williamson, C., Bauer, G., Enos, J., Arnold, G., Kramer, W., Becker, P., Doshi, A., D'Souza, C., Cummins, P., Laurier, F., Bojesen, M.: "ArcticDEM", [doi.org/10.7910/DVN/OHHUKH](https://doi.org/10.7910/DVN/OHHUKH), Harvard Dataverse, V1, 2018.
- 630 Sexton, J. O., Song, X. P., Feng, M., Noojipady, P., Anand, A., Huang, C., Kim, D. H., Collins, K. M., Channan, S., DiMiceli, C., and Townshend, J. R.: Global, 30-m resolution continuous fields of tree cover: Landsat-based rescaling of MODIS vegetation continuous fields with lidar-based estimates of error, *International Journal of Digital Earth*, 6(5):427–448, [doi.org/10.1080/17538947.2013.786146](https://doi.org/10.1080/17538947.2013.786146), 2013.
- Shaw, T. E., Gascoin, S., Mendoza, P. A., Pellicciotti, F., and McPhee, J.: Snow depth patterns in a high mountain Andean catchment from satellite optical tristereoscopic remote sensing, *Water Resources Research*, [doi/10.1029/2019WR024880](https://doi.org/10.1029/2019WR024880), 2019.
- 635 Shaw, T., Caro, A., Mendoza, P., Ayala, Á., Gascoin, S., and McPhee, J.: The Utility of Optical Satellite Winter Snow Depths for Initializing a Glacio-Hydrological Model of a High-Elevation, Andean Catchment, *Water Resources Research*, [doi.org/10.1029/2020WR027188](https://doi.org/10.1029/2020WR027188), 2020.
- 640 [Shean, D., Swinski, J. P., Smith, B., Sutterley, T., Ugarte, C., Lidwa, E., and Neumann, T.: SlideRule: Enabling rapid, scalable, open science for the NASA ICESat-2 mission and beyond. \*Journal of Open Source Software\*, 8, 1–6. <https://doi.org/10.21105/joss.04982>, 2023.](https://doi.org/10.21105/joss.04982)
- Shean, D.: High Mountain Asia 8-meter DEM Mosaics Derived from Optical Imagery, Version 1. Boulder, Colorado USA. NASA National Snow and Ice Data Center Distributed Active Archive Center, doi: [doi.org/10.5067/KXOVQ9L172S2](https://doi.org/10.5067/KXOVQ9L172S2), 2017.
- 645 Shean, D. E., Alexandrov, O., Moratto, Z. M., Smith, B. E., Joughin, I. R., Porter, C., and Morin, P.: An automated, open-source pipeline for mass production of digital elevation models (DEMs) from very-high-resolution commercial stereo satellite imagery, *ISPRS Journal of Photogrammetry and Remote Sensing*, 116:101–117, [doi.org/10.1016/j.isprsjprs.2016.03.012](https://doi.org/10.1016/j.isprsjprs.2016.03.012), 2016.
- 650 Smith, B., Fricker, H. A., Holschuh, N., Gardner, A. S., Adusumilli, S., Brunt, K. M., Csatho, B., Harbeck, K., Huth, A., Neumann, T., Nilsson, J., and Siegfried, M. R.: Land ice height-retrieval algorithm for NASA's ICESat-2 photon-counting laser altimeter, *Remote Sensing of Environment*, 233, [doi.org/10.1016/j.rse.2019.111352](https://doi.org/10.1016/j.rse.2019.111352), 2019.
- Sturm, M., Goldstein, M. A., and Parr, C.: Water and life from snow: A trillion dollar science question, *Water Resources Research*, 41(1):3534–3544, [doi.org/10.1002/2017WR020840](https://doi.org/10.1002/2017WR020840), 2017.
- 655 Treichler, D. and Käab, A.: Snow depth from ICESat laser altimetry — A test study in southern Norway, *Remote Sensing of Environment*, 191:389–401, [doi.org/10.1016/j.rse.2017.01.022](https://doi.org/10.1016/j.rse.2017.01.022), 2017.